applied sciences

MDPI

Article

Fatigue Effects on the Lower Leg Muscle Architecture Using Diffusion Tensor MRI

Filipa João [1,*], Sérgio Alves [2], Mário Secca [2], Michael Noseworthy [3] and António Veloso [1]

[1] CIPER, Faculdade de Motricidade Humana, Universidade de Lisboa, Estrada da Costa, Cruz-Quebrada-Dafundo, 1499-002 Oeiras, Portugal
[2] Departamento de Física, Cefitec, Faculdade de Ciências e Tecnologia, Universidade Nova de Lisboa, 2829-516 Caparica, Portugal
[3] Electrical and Computer Engineering, School of Biomedical Engineering, McMaster University, Hamilton, ON L8S 4L8, Canada
* Correspondence: filipajoao@fmh.ulisboa.pt

Abstract: Proton density (PD) and diffusion tensor imaging (DTI) are imaging techniques that enable the acquisition of data from living subjects that can be used in the fine-tuning of subject-specific models' architectural parameters. The aim of this study was to determine the in vivo 3D architectural parameters (volume, pennation angle, fiber length and physiological cross-sectional area) of the gastrocnemius medialis, gastrocnemius lateralis, soleus and tibialis anterior muscles using proton density and diffusion tensor imaging data before and after an exhaustive one-legged jump exercise. These methods were used in the in vivo 3D data acquisition of six young and physically active female subjects' lower legs, followed by a fiber-tracking algorithm and analysis tools. No significant differences were found in the muscles' architecture after the exercise, with the following exceptions: the anatomical cross-section area of the gastrocnemius medialis increased (p-value 0.001, effect size 0.18) after exercise; the fiber lengths of the gastrocnemius medialis, lateralis and soleus muscles were higher after exercise (p-value 0.002, 0.001 and 0.001, respectively, and effect size 2.03, 1.29 and 0.85, respectively); and the soleus mean pennation angle decreased after exercise (p-value 0.0015, effect size 2.31). These changes (or lack thereof) could be attributed to the extended acquisition time of the MRI scans to minimize noise: by increasing the acquisition time, the effect of the exercise may have been partially lost due to muscle recovery.

Keywords: calf muscles; biomechanics; cyclic exercise; imaging techniques; tractography

check for updates

Citation: João, F.; Alves, S.; Secca, M.; Noseworthy, M.; Veloso, A. Fatigue Effects on the Lower Leg Muscle Architecture Using Diffusion Tensor MRI. *Appl. Sci.* **2022**, *12*, 9767. https://doi.org/10.3390/app12199767

Academic Editor: Claudio Belvedere

Received: 26 August 2022
Accepted: 23 September 2022
Published: 28 September 2022

1. Introduction

The architecture of skeletal muscle, which is defined as the arrangement of muscle fibers relative to the axis of force generation [1], is the main determinant of the mechanical behavior of skeletal muscles [2,3]. Muscle fibers differ in their mechanical, histological, morphological, biochemical and biomechanical properties, allowing them to have different functionalities.

During force production, there are several important muscle architectural parameters to consider. Muscle architectural parameters, including muscle fiber length, physiological cross-sectional area (PCSA) and pennation angle (the angle between muscle fibers and the tendon plate), are associated with force production [4,5]. The anatomical cross-sectional area (ACSA) is simply the largest cross-section across the whole muscle, while the PCSA is the architectural parameter that is directly proportional to the maximum force generated by the muscle because it takes into account the pennation angle [6–9]. It is also the parameter that is most difficult to measure because its value is based on the entire muscle volume and includes the estimate of fiber length to reach the value for the area across the entire muscle [9]; therefore, it is indirectly determined from the muscle volume and muscle fiber length.

Computational models of the musculoskeletal system are widely used to study the mechanisms of musculoskeletal performance and to simulate specific conditions [10]. They were created based on anatomical data collected from cadaveric specimens. Models allow us to answer "what if" questions; isolate individual sources of input data; and estimate muscle parameters, such as muscle forces, that are difficult to measure experimentally [11,12]. To estimate the muscle volume or PCSA, the data of muscle force-generating capacities derived from cadaveric studies are often used to scale models of the muscle–tendon unit [10,13,14]. The use of those databases allows for a better understanding of general principles of muscle function, but the comparability to individual muscle performance remains unclear [15]. It is likely that data from cadaveric specimens do not accurately reflect the absolute or relative sizes of muscles in young and healthy subjects [16]. Moreover, cadaveric studies are usually based on a small number of specimens [17,18] and the fascicle length measured from each muscle are averaged in most cadaveric studies, and thus, muscle models usually assume that all fascicles within each muscle have the same length [19]. The same happens with the pennation angle: simulation models commonly assume muscle fibers to be one single structure with only one angle between the fiber's direction and the aponeurosis. Despite a valid and reliable 3D ultrasound technique for the assessment of the gastrocnemius medialis existing in the literature [20], no comprehensive ultrasound technique that allows for three-dimensionally measuring the architectural parameters of the anterior and posterior leg muscles exists. Therefore, this study used proton density and diffusion tensor imaging for 3D measurements of the leg muscles simultaneously [21]. Thus, the need to create accurate, individualized models of the musculoskeletal system is driving advances in imaging techniques, especially in magnetic resonance imaging (MRI) [22–24].

MRI is considered the most useful non-invasive imaging technique (although it is expensive and post-processing is laborious) that allows for the reconstruction of the whole muscle, enabling the quantification of detailed structure, function and metabolism from the muscle tissue [25]. MRI offers an abundance of novel methods for the acquisition of data from living subjects. One of those methods is diffusion tensor imaging (DTI) [26–29]. This imaging technique relies on the correspondence between cell geometry and the anisotropic nature of water diffusion in the muscle [28]. The theoretical basis for DTI states that the self-diffusion of water in tissue is restricted by membranes and other cellular constituents, resulting in an apparent diffusion coefficient, which is lower than the free diffusion coefficient and is orientation-dependent for elongated structures. Skeletal muscles are composed of fibers that have an elongated, generally cylindrical shape. The diffusion tensor can be described using a 3×3 matrix, and at least six independent directions for the diffusion gradients must be assessed to calculate the diffusion tensor. A proton density (PD)-weighted scan has its only signal change coming from the differences in the number of available spins (hydrogen nuclei in water). It uses a spin echo or a gradient echo sequence, with a short echo time and a long repetition time. PD images are useful for determining the muscle boundaries due to the elevated detail in the image, enabling the determination of the muscle cross-sectional area and subsequently muscle volume using simple image processing software.

Muscle volume is essential when evaluating muscle performance and functional consequences of changes in muscle size and strength due to training, aging or immobilization [15,30]. Most of the studies regarding these effects in muscle architecture were obtained through ultrasonography, which is limited to planar measurements and can only be used in superficial muscles. Moreover, when dealing with long muscle fibers, the length is not directly measured but is instead estimated via regression. These studies reported increases in muscle thickness and pennation angles of the vastus lateralis muscle following a leg press exercise [31], a cycloergometer test until exhaustion [32] or strength training programs [33,34]. Regarding the acute effects of exercise analyzed with MRI techniques, the following studies were reported: ankle plantarflexion exercises in the supine position with eccentric contractions showed changes in the gastrocnemius medialis (GM) values of FA, ADC and T2 after exercise [26]; during a walking exercise, followed by a 30 s dorsiflexion exercise, the ADC and T2 values of the tibialis anterior muscle (TA) increased [27]; another study showed that after isometric contraction of repeated plantar flexion and dorsal extension of the right ankle with a tiptoe position, the FA of soleus and MG muscles decreased but gradually recovered to the baseline after one week [35]; and another study showed that after a one-legged plantarflexion exercise, the CSA and T2 values of inactive muscles decreased, with no changes in ADC, and CSA, T2 and ADC values increased in the exercised leg [36].

Despite these results, the architectural muscle parameters that have a linear relationship with force production are still lacking in most of the research that uses this method. Regarding this, the aim of our study was to determine the in vivo 3D architectural parameters (volume, ACSA, pennation angle, fiber length and PCSA estimation) of the lower leg muscles using PD and DTI imaging data before and after an exhaustive unilateral jumping task. These methods were used in the in vivo 3D data acquisition of all the subjects' dominant lower legs, followed by a fiber-tracking algorithm with visualization and analysis tools. We hypothesized the following: (1) due to the fatigue effect and the amount of water content that would circulate in the body after the exercise bout, the muscle volume and cross-sectional areas would increase, as well as the pennation angle of the plantarflexor muscles, and (2) the shape of the analyzed muscles would not be different between subjects in both the pre- and post-exercise conditions.

2. Materials and Methods

2.1. Subjects

Six young female (age: 25.7 ± 5.2 years, mass: 61.0 ± 8.1 kg, height: 1.6 ± 0.1 m), healthy volunteers participated in this study. The inclusion criteria were as follows: age between 18 and 35, physically active with a minimum of 3 days/week of training sessions (any type of exercise) and able to perform a jumping cyclic exercise in one leg. The exclusion criteria were as follows: have any history of lower extremity injury or surgery in the last 12 months, have any kind of pain and have any limitations in performing an MRI exam. Informed consent was given by each subject prior to testing and the work was approved by the Ethical Committee of the Faculty of Human Kinetics, University of Lisbon.

2.2. Experimental Setup

All the subjects were examined in a 1.5 T whole-body MRI scanner (Signa HDxT 1.5T, GE Healthcare, Chicago, IL, USA) before and immediately after the exercise protocol. A pelvic coil was used for all the measurements. This coil was used instead of an extremity coil because we wanted to scan the entire lower leg from the femoral condyles to the calcaneus so that we could measure the entire muscle length (Figure 1-right).

Figure 1. (**Left**) Subject in the supine position with the leg in the custom-made structure, which avoided compression of the leg muscles against the MRI table. (**Right**) The leg with the pelvic coil.

Leg immobilization was carried out by using a custom-made structure, which was made of a nonmagnetic material, adjustable to the subject's leg length and avoided compression of the leg muscles against the MRI table (Figure 1-left). This structure was fixed to the table and the subjects kept their foot and leg in the same position, completely relaxed, guaranteeing the same reference frame in all the MRI acquisitions (before and after the exercise protocol). Subjects were placed in the supine position with their feet first and care was taken to position the subjects with the long axis of the leg placed parallel to the magnetic field. The following imaging protocol was performed: first, proton density and diffusion tensor images were acquired from the dominant lower leg at rest. Afterward, the subjects performed the exercise protocol. Finally, new imaging sequences were then immediately acquired in the order of DTI and PD. The images were acquired using the following parameters: for DTI, 60 axial acquisitions, gradient-echo sequence, TE = 35, TR = 3622 and slice thickness = 3.9 mm; for proton density: 54 axial acquisitions with a turbo spin-eco gradient, TE = 7.6 and TR = 4140.

2.3. Exercise Protocol

To recruit the ankle plantar flexors, this study adopted a simple exercise task that the subjects were able to perform near the MRI room without any specific equipment besides regular training shoes. After the first bout of MRI scans, the subjects were asked to perform a sequence of one-legged jumps, keeping their hands on their waist. They constantly received verbal encouragement to keep performing the exercise despite the fatigue increasing. The end of the task was considered when the subject could not take the entire foot from the floor anymore (the total exercise time was 1 m 30 s on average). Immediately after the exercise, the subject was placed on the MRI table again, with the exercised leg positioned on the top of the leg fixation structure and the same bout of imaging sequences was collected.

2.4. Image Analysis and Data Processing

Regions of interest (ROIs) were drawn in the PD images using a piecewise linear boundary provided by the Osirix software version 9.0, Pixmeo SARL (Bernex, Switzerland) (Figure 2-left). The ROIs were outlined manually according to the anatomical boundaries of the tibialis anterior (TA), gastrocnemius medialis (GM), gastrocnemius lateralis (GL) and soleus (SOL) muscles. All the ROIs were manually drawn by the same operator, with a total of 46–82 contour curves for each muscle on each phase of the protocol (before and after the exercise). The volumes of the individual muscles (V_m) were determined by summing the product of the cross-sectional areas of the muscle from each image and the slice thickness (3.9 mm) (Figure 2-right). Moreover, from the PD images, the maximal anatomical cross-sectional area ($ACSA_{max}$) was determined as the largest cross-section outlined across the whole muscle. Muscle length (L_m) was defined as the distance between the muscle's proximal and distal ends.

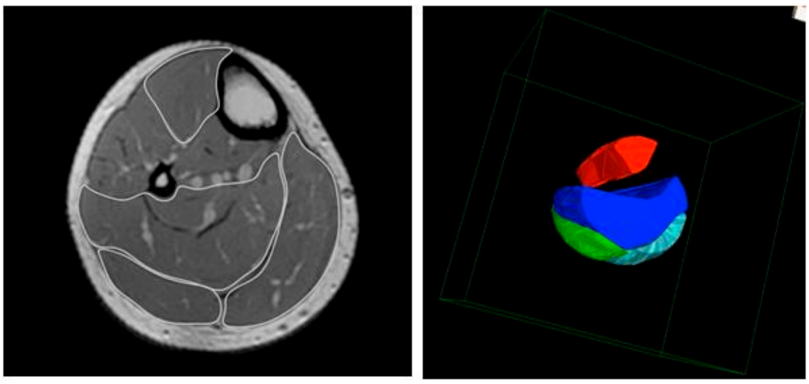

Figure 2. (**Left**) Boundaries of the GM, GL, SOL and TA muscles, which were delimited in the DP images. (**Right**) Muscles' volumes computed with the ACSA determined in each slice of each muscle.

The three principal axes of the diffusion tensor can be calculated through a diagonalization process, where the eigenvalues and eigenvectors are determined. These parameters give us information regarding the shape and the direction of the diffusion, respectively [25]. Other parameters, derived from these, can be quantified: the fractional anisotropy (FA) and the apparent diffusion coefficient (ADC). The computation of the diffusion tensor imaging results was performed through a custom script that used FSL Tools (FMRIB Analysis Group, Oxford, UK) developed to process the imaging data. This routine included the motion and eddy current correction and the co-registration of the PD images with the diffusion tensor images. Fibers were tracked from the diffusion tensor using the free software Diffusion Toolkit version 0.6.2 and TrackVis version 0.5.2 (Ruopeng Wang, Van J. Wedeen, Athinoula A. Martinos, Center for Biomedical Imaging, Department of Radiology, Massachusetts General Hospital, Boston, MA, USA). The DTI data was opened in TrackVis and the anatomical image (PD) was superimposed on the DTI. The slice corresponding to the $ACSA_{max}$ of each muscle was chosen to draw the seed ROI necessary for the tracking. Two more ROIs were drawn, four slices above and four slices below, to guarantee the tracking of fibers only from that specific muscle. From the tracked fibers, the following parameters were determined: the average fiber length (L_f), defined as the mean value of the length of the fibers calculated through the tracking algorithm in Diffusion Toolkit, and the pennation angle (θ), defined as the fiber angle relative to the force-generating axis. It was measured directly in the fiber-tracked images (using Osirix software) by rotating the image in line with the longitudinal axis and positioning it in a plane where it visualized the preferred angular orientation of the fibers (Figure 3). When two or more fiber orientations were visualized, all the angles were determined, and the mean value was used in the results.

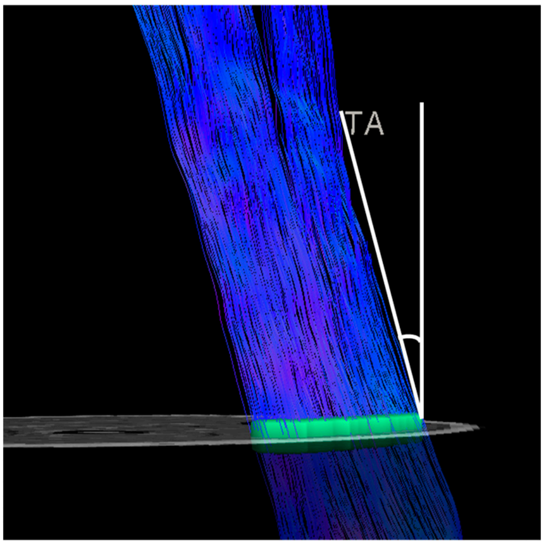

Figure 3. Calculation of the pennation angle for the TA muscle.

PCSA is directly proportional to the maximum titanic tension that can be generated by the muscle and represents the sum of the cross-sectional areas of all the muscle fibers within the muscle. It was estimated using Equation (1), which was derived from the work of the pioneer Gans [37] and continued nowadays by Lieber [38].

$$\text{PCSA (cm}^2\text{)} = (\text{muscle volume (cm}^3\text{)})/(\text{fiber length (cm)}) \cdot \cos\theta, \tag{1}$$

The inter-subject variability regarding the shape of the muscles was also investigated. Following Albracht's [15] theoretical consideration, which is also related to the muscle volume of the triceps surae muscles, in Equation (2), the general muscle volume (V_m) is given as a fraction of the product of $ACSA_{max}$ and L_m.

$$V_m = p \cdot ACSA_{max} \cdot L_m, \tag{2}$$

where p is defined as the muscle shape factor, which can vary between 0 and 1. In general, it is assumed that the muscle shape is the same across the population, but to test whether it is valid to make this assumption within our group of subjects, we considered the intersubject variability by measuring the coefficient of variance (CV) of three ratios: the ratio between V_m and the product of $ACSA_{max}$ and L_m (shape factor p), as well as the ratio between V_m and either the $ACSA_{max}$ or L_m for the four muscles mentioned above.

2.5. Statistical Analysis

The normality of the variables was tested and a paired-sample t-test analysis was used to compare the differences between the architectural parameters before and after the exercise task. A post hoc analysis of the sample power was calculated for this study using G-Power (version 3.1; Franz Faul, Universität Kiel, Germany) for a medium effect size (0.5), $\alpha = 0.05$ and a sample of 6 participants, the resulting power was 0.2. Moreover, an online tool was used to calculate the effect size for a paired samples *t*-test (Cohen's d_z). Afterward, Excel software (Microsoft Corporation, Redmond, WA, USA) was used to calculate the Hedges' (adjusted) g effect size, which includes an adjustment for sample sizes of less than 20 subjects [39], to estimate the magnitude of the effects of the exercise on the results of the muscle architectural parameters. The statistical significance was set at the level of $p < 0.05$. All the statistical tests were performed using SPSS Statistics software (version 22.0; IBM, Chicago, IL, USA).

3. Results

Regarding the results, Table 1 shows the architectural parameters obtained for the GM, GL, SOL and TA muscles in the two conditions: pre- and post-exercise. The corrected effect sizes of these results are reported in Table 2.

Table 1. Mean values ± SDs of the muscle architectural parameters of the GM, GL, SOL and TA muscles determined using the imaging techniques PD and DTI pre- and post-exercise. The length of the muscle was the same in the two conditions.

	V_m (cm^3)		$ACSA_{max}$ (cm^2)		L_m (cm)	L_f (cm)		PCSA (cm^2)		Pennation Angle (°)	
	Pre	Post	Pre	Post		Pre	Post	Pre	Post	Pre	Post
GM	189.4 ± 56.3	193.6 ± 54.8	14.0 ± 4.0	14.4 ± 4.1 *	23.1 ± 1.8	6.3 ± 0.5	7.0 ± 0.3 *	28.3 ± 7.9	26.6 ± 8.2	18.1 ± 2.1	17.9 ± 2.0
GL	96.1 ± 28.5	100.2 ± 29.7	8.3 ± 1.8	8.8 ± 2.4	20.3 ± 1.7	5.8 ± 1.6	7.2 ± 1.0 *	16.9 ± 5.8	13.7 ± 4.1	11.3 ± 2.2	13.7 ± 3.1
SOL	369.2 ± 66.5	370.2 ± 62.9	24.9 ± 4.2	25.0 ± 4.1	29.9 ± 1.2	5.6 ± 0.9	6.1 ± 0.7 *	59.7 ± 5.6	56.4 ± 4.3	25.7 ± 1.3	20.4 ± 3.0 *
TA	110.9 ± 22.8	109.3 ± 21.4	8.1 ± 1.4	7.9 ± 1.2	27.8 ± 2.4	9.3 ± 0.5	9.5 ± 0.9	9.5 ± 2.1	9.3 ± 1.4	19.7 ± 2.9	16.8 ± 2.7

* Significant difference (*p*-value < 0.05).

Table 2. Corrected effect sizes (Hedges's g) of the changes reported in Table 1 regarding the architectural parameters from the GM, GL, SOL and TA muscles.

	Vm (cm^3) Hedges's g	**$ACSA_{max}$ (cm^2) Hedges's g**	**L_f (cm) Hedges's g**	**PCSA (cm^2) Hedges's g**	**Pennation Angle (°) Hedges's g**
GM	0.09	0.18	2.03	0.30	0.14
GL	0.17	0.32	1.29	0.83	0.17
SOL	0.18	0.04	0.85	0.90	2.31
TA	0.10	0.22	0.31	0.18	1.48

Neither muscle volume nor $ACSA_{max}$ demonstrated statistically significant differences after the exercise, except for the GM $ACSA_{max}$, which increased significantly in the post-exercise condition. However, the small effect size revealed that for a randomly selected person, the chance to increase the GM $ACSA_{max}$ after a bout of cyclic exercise was quite modest. The results showed that the SOL was the muscle with higher volume, followed by the GM, the TA and the GL. The $ACSA_{max}$ was higher for the SOL, GM and GL, and lower for the TA. Regarding the total length of the muscle, the longer muscle was the

SOL, reaching almost 30 cm, followed by the TA, GM and GL muscles. Regarding the pennation angle, it was verified that different portions of the muscle fibers had different pennation angles, especially for the SOL muscle. The preferential directions were assessed, although only the mean of those angles is reported. It was assumed that there was only one pennation angle per muscle. The highest pennation angle was found in the SOL muscle, followed by the TA, GM and GL muscles. After the exercise, only the pennation angle of the SOL muscle revealed a significant decrease. It was also the muscle where the effect size was greater. The fiber length was assessed with the fiber-tracking process, and the mean length of all the muscle fibers is reported in Table 1. The longest fibers were observed in the TA muscle, followed by the SOL, GL and GM muscles. After the exercise, the GM, GL and SOL muscles showed significant increases in fiber length. These results led us to a discussion concerning the fiber-tracking method itself, which is better explored in the Discussion section. The PCSA was estimated using Equation (1) using the measured data V_m, L_f and pennation angle. We observed that the SOL muscle had the highest PCSA, followed by the GM, GL and TA. After the exercise, no significant changes were observed. The results for the inter-subject variability regarding muscle shape are presented in Table 3, and Figure 4 shows the results for the individual parameters. The ratio between V_m and L_m was the one where the individuals were more distant from the mean result of muscle shape (the CV% had the highest results). On the other hand, the ratio between V_m and the product of $ACSA_{max}$ and L_m showed the lowest CV%, which may be a good indicator that the shape of the muscles was similar between subjects. The lower the CV%, the lower the variability.

Table 3. Mean values ± SDs and the coefficient of variance (in %) of the ratio between V_m and the product of $ACSA_{max}$ and L_m, the ratio between V_m and $ACSA_{max}$, and the ratio between V_m and L_m for the GM, GL, SOL and TA muscles.

	$V_m/(ACSA_{max} \cdot L_m)$				$V_m/ACSA_{max}$				V_m/L_m			
	Pre		Post		Pre		Post		Pre		Post	
	Mean	CV	Mean	CV	Mean	CV	Mean	CV	Mean	CV	Mean	CV
GM	0.59 + 0.04	7.5	0.59 + 0.05	8.6	13.50 ± 0.86	6.3	13.50 ± 1.29	9.5	8.23 ± 2.43	29.6	8.40 ± 2.35	27.9
GL	0.56 ± 0.03	5.1	0.56 ± 0.05	8.5	11.32 ± 1.26	11.2	11.28 ± 1.18	10.5	4.68 ± 1.13	24.2	4.87 ± 1.12	23.0
SOL	0.49 ± 0.03	5.3	0.49 ± 0.02	4.2	14.77 ± 0.91	6.1	14.79 ± 0.69	4.6	12.31 ± 2.08	16.9	12.29 ± 1.98	16.1
TA	0.50 ± 0.04	7.3	0.50 ± 0.02	4.2	13.76 ± 0.96	7.0	13.78 ± 0.78	5.6	3.96 ± 0.53	13.4	3.91 ± 0.50	12.8

Within each muscle of the leg, and in both conditions, the CV was the lowest (4.2–8.6%) for the ratio between V_m and the product of $ACSA_{max}$ and L_m, followed by the ratio between V_m and $ACSA_{max}$ (4.6–11.2%). The ratio between V_m and L_m had the highest CV (12.8–29.6%).

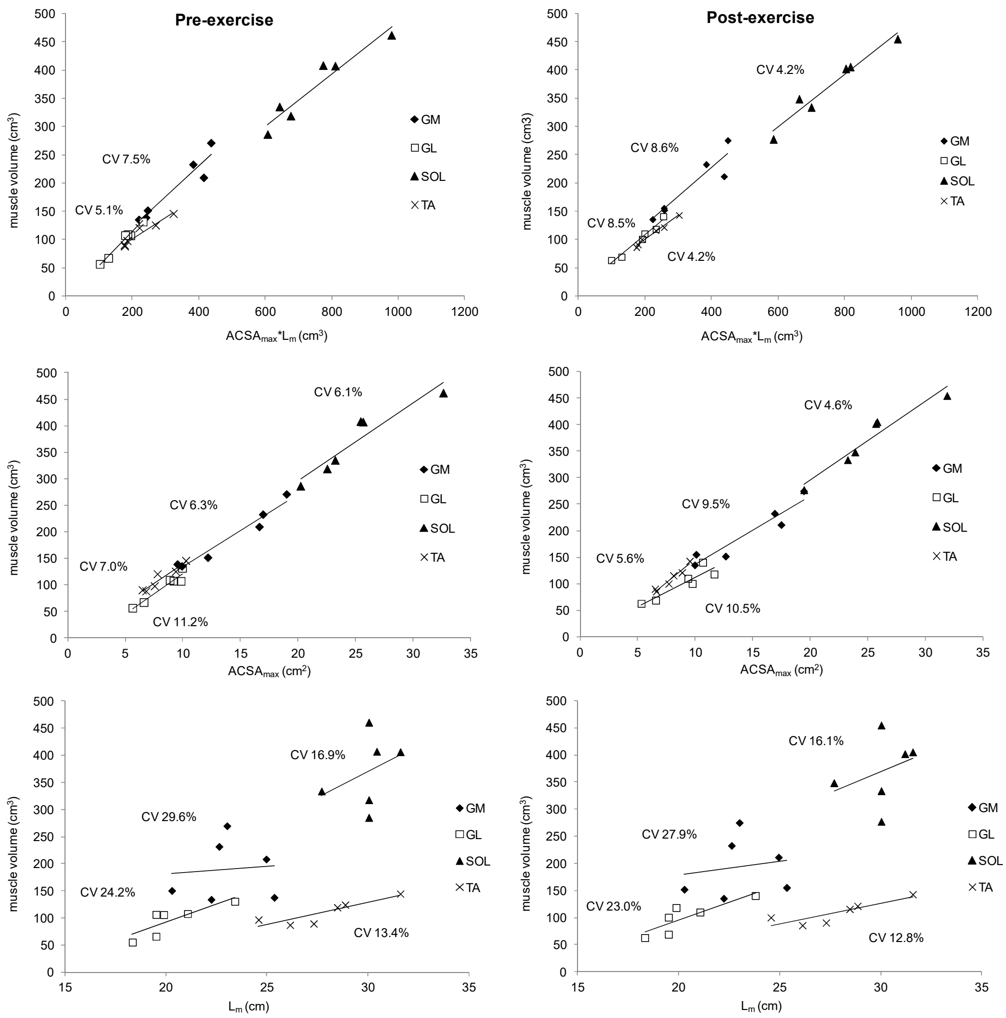

Figure 4. Inter-subject variability regarding muscle shape. Measured values for the muscle volume and the product of $ACSA_{max}$ and muscle length (**first line**), ACSAmax (**second line**) and muscle length (**third line**) before and after the exercise. The values for the CV are presented near the regression lines and also in Table 3.

4. Discussion

The aim of this study was to determine the architectural parameters of the human lower leg muscles (volume, $ACSA_{max}$, muscle length, pennation angle, PCSA and fiber length) using quantitative variables that were provided by diffusion tensor and anatomical MRI data. To accomplish this, the process started with the visualization and delimitation of ROIs corresponding to each muscle in each slice of a DP image scan. Afterward, the maximal ACSA and the length of the muscle were assessed, followed by a fiber-tracking algorithm that mapped the diffusion tensor, allowing for the reconstruction of the muscle fibers and subsequent estimation of fiber length, pennation angles and PCSA.

For the second aim of this study, we ascertained whether short-term exhaustive stretch–shortening cycle exercise would induce changes in these muscle architecture parameters and whether DTI could be used to study acute muscular responses to exercise.

The muscle volume did not change significantly after the acute exercise, although the increased water content in exercising muscles is known to affect both extra- and intra-cellular volumes [40,41]. One of the reasons for this unchanged result may have been the time between the end of the exercise and the duration of the scan protocol. Due to the rapid decay of the DTI signal, the DP scan was performed only after the DTI scan. It is possible that the recovery of muscles occurred rapidly and when drawing the muscles' boundaries to calculate the muscle volume, the anatomical images did not reveal significant differences. Nevertheless, quantifying the muscle volume allowed us to quantify a subject-specific architectural parameter, which was needed to calculate an individual's PCSA. The manual segmentation of the muscles from the MRI images is an arduous process when automatic routines are not used. As a manual process, the delimitation of the muscle contours was subject to error, especially in the images where the muscle boundaries were not well defined. Nevertheless, that task was always performed by the same operator. Advanced post-processing approaches that are designed for musculoskeletal modeling will further improve the efficiency of extracting muscle anatomy from MR images.

Muscle models generally assume that the pennation angle is constant across all fibers. In accordance with other imaging studies [29,42], we verified that fibers from the same muscle had different pennations (and we used the mean value to calculate the muscles' PCSA). By creating a tridimensional representation of muscle fibers, we could add information that may help us to surpass the limitation of representing muscles as single line segments that remain unchanged in terms of shape when interacting with the underlying bones and other structures [22]. These observations strengthen the fact that muscle models should consider this parameter and use more than one single line segment to characterize the muscle structure. However, we observed that the different angles measured in the tracked fibers did not significantly alter the value of the PCSA. In fact, from all the architectural parameters, the pennation angle probably has a small influence on muscle PCSA calculations and, thus, in predicting the maximum muscle force [9]. After exercise, the pennation angle significantly decreased in the SOL muscle. This change may have been attributed to the challenging determination of the pennation angles in this particular muscle due to its multipennate architecture. It is quite difficult to determine all the preferential directions of the tracts and, of course, the mean value does not exactly show the individual fiber pennations. An increase in the pennation angles of the most contributing muscles (plantarflexors) was expected but no significant changes were verified. These results showed that we did not entirely verify our first hypothesis, particularly regarding muscle volume and muscle cross-section areas variables.

The tractography process enables the quantification of the length of the muscle fiber. Fiber length is a muscle parameter that is commonly estimated using ultrasonographic equipment [32,43–45]. Ultrasonography and reconstruction methods have been widely used to determine not just fiber length but also pennation angles; however, they do not take into account the spatial variation and orientation of the muscle fibers. Ultrasonography is easier to use, faster and cheaper, but is limited to planar measurements and can only be used in superficial muscles. Moreover, when dealing with long muscle fibers, the length is not directly measured but is instead estimated via regression. Muscle fiber length can only be rigorously determined via the microdissection of individual fibers from the fixed tissues [46]. Additionally, the effects of exercise interventions on muscle fiber length measurements can vary between ultrasound assessments and extrapolation methods due to a lacking gold standard method for muscle fiber length measurement [47]. Another advantage of DTI is the ability to measure both fiber length and pennation angle through the mapping of the eigenvalues from the diffusion tensor, which gives us the direction of the fibers. The mapping of the diffusion tensor allows for the reconstruction of the muscle fibers (and subsequent estimation of the fiber length), assuming that there is a preferential direction for the water to diffuse across the muscle cells. We observed that the lengths of the fibers estimated through this process were higher than the ones reported in the literature regarding cadavers or live subject experiments. Despite the advantages of the DTI measurement, a gold standard for muscle fiber length measurements has not yet been defined, which might be a limitation of this study. After the exercise task, the length of the fibers significantly increased for the plantarflexors SOL, GM and GL. We believe that the increase in the water content that circulates inside the cells will facilitate water diffusion. Increasing the space between the microstructures may have increased diffusion in all the directions of the tissue as a consequence. This lower restriction of the diffusion in the longitudinal axis of the fibers may justify the increase in the "apparent" length of the fibers.

Having this in mind, the "apparent" length of the fibers before the exercise may have been underestimated since the probability of the tracking being discontinued was much higher. Moreover, different stop criteria settings changed the resulting fiber length. We used the default curvature settings > 20°. We must still interpret these results with caution, as no study of the reliability and sensitivity of the method was performed, which is one of the limitations of the study.

Compared with the existing literature data from cadaveric studies [18], our results for the pennation angle showed higher values for TA (almost twice the pennation) and similar values for the other muscles. Compared with in vivo studies using ultrasonography, we found similar results for the anterior angle of pennation of the MG muscle, as well as for the posterior angle of pennation for the GL muscle and for both compartments analyzed for the posterior soleus muscle reported by Martin and colleagues [48]. Regarding muscle length, our values were smaller for the four muscles (less than 1 cm) when compared with the same cadaveric database and also with the subjects assessed by Albracht et al. [15] using ultrasonography. However, our sample was a group of young females with different anthropometric characteristics and smaller segments. The PCSA estimated revealed much smaller values when compared with the existing literature (although the SOL and TA PCSAs were similar to those assessed in cadavers). We could attribute this to the estimated fiber length, which may have been overestimated (both before and after exercise). Moreover, some of the differences found may be partially explained by the fact that cadaveric tissue is subjected to specific protection procedures before experimental studies and the effects of those actions are still not well understood. Moreover, rigor mortis can produce a slow contraction in the skeletal muscle [49], with consequent effects on the fiber architecture.

To test our second hypothesis, namely, the shape of the muscle was the same within our group of subjects, we considered the inter-subject variability by measuring the CV of the ratio between V_m and the product of $ACSA_{max}$ and L_m (shape factor p), as well as the ratio between V_m and either the $ACSA_{max}$ or L_m for the four muscles. We found that, similar to Albracht et al. [15], the lowest inter-subject variability occurred for the ratio between V_m and the product of $ACSA_{max}$ and L_m, demonstrating that the shape of each muscle seemed to be similar across the examined subjects.

Other limitations regarding this study must be reported. Regarding the use of DTI to assess the changes in the muscle architecture immediately after exercise, an important issue should be raised: the transverse relaxation time in muscles is short. This means that the signal-to-noise ratio was limited, thus increasing the number of averages needed to minimize the noise, thereby extending the acquisition time [22]. By increasing the acquisition time, the effect of the exercise may be partially lost due to a fast recovery period. This may explain some of our results since no significant changes were observed in most of the muscle's architecture. Moreover, it might be a limitation of this study that proton density and diffusion tensor imaging for 3D measurements of the leg muscles' architectural parameters does not entirely show a very high intraclass correlation coefficient for all muscle architectural parameters [21], and thus, we should be careful when interpreting the results. Additionally, the small sample size and the fact that the participants were only female subjects may also decrease the external validity of this study, making it difficult to extrapolate the results to other populations.

The relationship between the structure and function of muscles is critical to understanding the physiological basis of force production and movement, especially in adaptive conditions, such as training, detraining, disease, age and immobilization, where the architecture of the muscle can undergo changes [50–53]. This relationship is usually studied through musculoskeletal models, where the anatomical and architectural parameters of the muscles are usually simplified and/or adapted from cadaveric databases, most of them with a small sample size [18]. Structural and functional parameters provided by PD and DTI, such as the trace of the diffusion tensor, allow for the non-invasive and in vivo measurement of critical parameters for the elaboration of those models, such as muscle volume, fiber length and PCSA. Adding these architectural parameters in the elaboration of those models may help us to accurately assemble subject-specific simulations to study human movement. This combination of advanced imaging techniques with computation methods will allow for the creation of more individualized models, and subsequently, estimation of muscle forces during specific movement patterns.

5. Conclusions

This study indicated that DTI is a viable non-invasive tool for assessing muscle architecture, specifically muscle volume, fiber length, PCSA and pennation angle. Muscle architecture has a considerable influence on the mechanical properties of the muscle–tendon complex, thus being crucial in force production. The use of imaging techniques, such as DTI, is an important advance in the study of human muscle architecture, promoting the integration of subject-specific parameters into musculoskeletal models as a replacement for cadaveric-based data. Regarding the use of DTI immediately after exercise, care should be taken because by increasing the acquisition time, the effect of the exercise may be partially lost during the scan.

Author Contributions: Conceptualization, F.J. and A.V.; methodology, F.J., S.A., M.S., M.N. and A.V.; software, F.J., S.A. and M.S.; validation, F.J., M.N. and A.V.; formal analysis, F.J. and A.V.; investigation, F.J., S.A. and A.V.; resources, M.S. and A.V.; data curation, F.J., S.A., M.S., M.N. and A.V.; writing—original draft preparation, F.J. and S.A.; writing—review and editing, F.J., S.A., M.S. and A.V.; visualization, F.J., S.A. and A.V.; supervision, A.V.; project administration, A.V.; funding acquisition, A.V. and F.J. All authors have read and agreed to the published version of the manuscript.

Funding: This research was funded by Fundação para a Ciência e Tecnologia (FCT) with the grants SFRH/BD/36318/2007 and PTDC/DES/103178/2008 through CIPER (unit 369447).

Institutional Review Board Statement: The study was conducted in accordance with the Declaration of Helsinki and executed in accordance with the Faculty of Human Kinetics Ethics Committee.

Informed Consent Statement: Informed consent was obtained from all subjects involved in the study.

Data Availability Statement: All data generated or analyzed during this study are included in this published article.

Acknowledgments: The authors would like to thank Cristina Menezes from Ressonância Magnética—Caselas, Lisbon, Portugal, for all the technical support during the data collection.

Conflicts of Interest: The authors declare no conflict of interest.

References

1. Lieber, R.L.; Friden, J. Clinical Significance of Skeletal Muscle Architecture. *Clin. Orthop. Relat. Res.* **2001**, *383*, 140–151. [CrossRef] [PubMed]
2. Lieber, R.L. Skeletal Muscle Adaptability. I: Review of Basic Properties. *Dev. Med. Child Neurol.* **1986**, *28*, 390–397. [CrossRef] [PubMed]
3. Lieber, R.L. Muscle Fiber Length and Moment Arm Coordination during Dorsi- and Plantarflexion in the Mouse Hindlimb. *Cells Tissues Organs* **1997**, *159*, 84–89. [CrossRef]
4. Yagiz, G.; Akaras, E.; Kubis, H.-P.; Owen, J.A. The Effects of Resistance Training on Architecture and Volume of the Upper Extremity Muscles: A Systematic Review of Randomised Controlled Trials and Meta-Analyses. *Appl. Sci.* **2022**, *12*, 1593. [CrossRef]
5. Shida, N.; Yagiz, G.; Yamada, T. The Effects of Exergames on Muscle Architecture: A Systematic Review and Meta-Analysis. *Appl. Sci.* **2021**, *11*, 10325. [CrossRef]
6. Fukunaga, T.; Ichinose, Y.; Ito, M.; Kawakami, Y.; Fukashiro, S. Determination of Fascicle Length and Pennation in a Contracting Human Muscle in Vivo. *J. Appl. Physiol.* **1997**, *82*, 354–358. [CrossRef]
7. Fukunaga, T.; Kawakami, Y.; Kuno, S.; Funato, K.; Fukashiro, S. Muscle Architecture and Function in Humans. *J. Biomech.* **1997**, *30*, 457–463. [CrossRef]
8. Haxton, H.A. Absolute Muscle Force in the Ankle Flexors of Man. *J. Physiol.* **1944**, *103*, 267–273. [CrossRef]
9. Lieber, R.L. *Skeletal Muscle Structure, Function & Plasticity—The Physiological Basis of Rehabilitation*; Lippincott Williams & Wilkins: Baltimore, MD, USA, 2002.
10. Delp, S.L.; Loan, J.P.; Hoy, M.G.; Zajac, F.E.; Topp, E.L.; Rosen, J.M. An Interactive Graphics-Based Model of the Lower Extremity to Study Orthopaedic Surgical Procedures. *IEEE Trans. Biomed. Eng.* **1990**, *37*, 757–767. [CrossRef]

11. Hamner, S.R.; Seth, A.; Delp, S.L. Muscle Contributions to Propulsion and Support during Running. *J. Biomech.* **2010**, *43*, 2709–2716. [CrossRef]
12. Delp, S.L.; Anderson, F.C.; Arnold, A.S.; Loan, P.; Habib, A.; John, C.T.; Guendelman, E.; Thelen, D.G. OpenSim: Open-Source Software to Create and Analyze Dynamic Simulations of Movement. *IEEE Trans. Biomed. Eng.* **2007**, *54*, 1940–1950. [CrossRef] [PubMed]
13. Anderson, F.C.; Pandy, M.G. A Dynamic Optimization Solution for Vertical Jumping in Three Dimensions. *Comput. Methods Biomech. Biomed. Eng.* **1999**, *2*, 201–231. [CrossRef] [PubMed]
14. Bobbert, M.F. Dependence of Human Squat Jump Performance on the Series Elastic Compliance of the Triceps Surae: A Simulation Study. *J. Exp. Biol.* **2001**, *204*, 533–542. [CrossRef] [PubMed]
15. Albracht, K.; Arampatzis, A.; Baltzopoulos, V. Assessment of Muscle Volume and Physiological Cross-Sectional Area of the Human Triceps Surae Muscle in Vivo. *J. Biomech.* **2008**, *41*, 2211–2218. [CrossRef]
16. Tate, C.M.; Williams, G.N.; Barrance, P.J.; Buchanan, T.S. Lower Extremity Muscle Morphology in Young Athletes: An MRI-Based Analysis. *Med. Sci. Sports Exerc.* **2006**, *38*, 122–128. [CrossRef]
17. Friederich, J.A.; Brand, R.A. Muscle Fiber Architecture in the Human Lower Limb. *J. Biomech.* **1990**, *23*, 91–95. [CrossRef]
18. Wickiewicz, T.L.; Roy, R.R.; Powell, P.L.; Edgerton, V.R. Muscle Architecture of the Human Lower Limb. *Clin. Orthop. Relat. Res.* **1983**, *179*, 275–283. [CrossRef]
19. Zajac, F.E.; Gordon, M.E. Determining Muscle's Force and Action in Multi-Articular Movement. *Exerc. Sport Sci. Rev.* **1989**, *17*, 187–230.
20. Weide, G.; van der Zwaard, S.; Huijing, P.A.; Jaspers, R.T.; Harlaar, J. 3D Ultrasound Imaging: Fast and Cost-Effective Morphometry of Musculoskeletal Tissue. *J. Vis. Exp. JoVE* **2017**, 55943. [CrossRef]
21. Bolsterlee, B.; D'Souza, A.; Herbert, R.D. Reliability and Robustness of Muscle Architecture Measurements Obtained Using Diffusion Tensor Imaging with Anatomically Constrained Tractography. *J. Biomech.* **2019**, *86*, 71–78. [CrossRef]
22. Blemker, S.S.; Asakawa, D.S.; Gold, G.E.; Delp, S.L. Image-Based Musculoskeletal Modeling: Applications, Advances, and Future Opportunities. *J. Magn. Reason. Imaging* **2007**, *25*, 441–451. [CrossRef] [PubMed]
23. Aeles, J.; Bolsterlee, B.; Kelp, N.Y.; Dick, T.J.M.; Hug, F. Regional Variation in Lateral and Medial Gastrocnemius Muscle Fibre Lengths Obtained from Diffusion Tensor Imaging. *J. Anat.* **2022**, *240*, 131–144. [CrossRef] [PubMed]
24. Franchi, M.V.; Raiteri, B.J.; Longo, S.; Sinha, S.; Narici, M.V.; Csapo, R. Muscle Architecture Assessment: Strengths, Shortcomings and New Frontiers of in Vivo Imaging Techniques. *Ultrasound Med. Biol.* **2018**, *44*, 2492–2504. [CrossRef]
25. Noseworthy, M.D.; Davis, A.D.; Elzibak, A.H. Advanced MR Imaging Techniques for Skeletal Muscle Evaluation. *Semin. Musculoskelet. Radiol.* **2010**, *14*, 257–268. [CrossRef]
26. Yanagisawa, O.; Kurihara, T.; Kobayashi, N.; Fukubayashi, T. Strenuous Resistance Exercise Effects on Magnetic Resonance Diffusion Parameters and Muscle-Tendon Function in Human Skeletal Muscle. *J. Magn. Reason. Imaging* **2011**, *34*, 887–894. [CrossRef]
27. Yanagisawa, O.; Shimao, D.; Maruyama, K.; Nielsen, M. Evaluation of Exercised or Cooled Skeletal Muscle on the Basis of Diffusion-Weighted Magnetic Resonance Imaging. *Eur. J. Appl. Physiol.* **2009**, *105*, 723–729. [CrossRef]
28. Heemskerk, A.M.; Sinha, T.K.; Wilson, K.J.; Ding, Z.; Damon, B.M. Repeatability of DTI-Based Skeletal Muscle Fiber Tracking. *NMR Biomed.* **2010**, *23*, 294–303. [CrossRef]
29. Heemskerk, A.M.; Sinha, T.K.; Wilson, K.J.; Ding, Z.; Damon, B.M. Quantitative Assessment of DTI-Based Muscle Fiber Tracking and Optimal Tracking Parameters. *Magn. Reason. Med.* **2009**, *61*, 467–472. [CrossRef] [PubMed]
30. Kawakami, Y.; Lieber, R. Interaction between Series Compliance and Sarcomere Kinetics Determines Internal Sarcomere Shortening during Fixed-End Contraction. *J. Biomech.* **2000**, *33*, 1249–1255. [CrossRef]
31. Csapo, R.; Alegre, L.M.; Baron, R. Time Kinetics of Acute Changes in Muscle Architecture in Response to Resistance Exercise. *J. Sci. Med. Sport* **2011**, *14*, 270–274. [CrossRef]
32. Brancaccio, P.; Limongelli, F.M.; D'Aponte, A.; Narici, M.; Maffulli, N. Changes in Skeletal Muscle Architecture Following a Cycloergometer Test to Exhaustion in Athletes. *J. Sci. Med. Sport* **2008**, *11*, 538–541. [CrossRef] [PubMed]
33. Alegre, L.M.; Jimenez, F.; Gonzalo-Orden, J.M.; Martin-Acero, R.; Aguado, X. Effects of Dynamic Resistance Training on Fascicle Length and Isometric Strength. *J. Sports Sci.* **2006**, *24*, 501–508. [CrossRef]
34. Blazevich, A.J.; Cannavan, D.; Coleman, D.R.; Horne, S. Influence of Concentric and Eccentric Resistance Training on Architectural Adaptation in Human Quadriceps Muscles. *J. Appl. Physiol.* **2007**, *103*, 1565–1575. [CrossRef] [PubMed]
35. Okamoto, Y.; Kunimatsu, A.; Miki, S.; Shindo, M.; Niitsu, M.; Minami, M. Fractional Anisotropy Values of Calf Muscles in Normative State after Exercise: Preliminary Results. *Magn. Reason. Med. Sci.* **2008**, *7*, 157–162. [CrossRef]
36. Nygren, A.T.; Kaijser, L. Water Exchange Induced by Unilateral Exercise in Active and Inactive Skeletal Muscles. *J. Appl. Physiol.* **2002**, *93*, 1716–1722. [CrossRef] [PubMed]
37. Gans, C.; Bock, W.J. The Functional Significance of Muscle Architecture—A Theoretical Analysis. *Ergeb. Anat. Entwickl.* **1965**, *38*, 115–142.
38. Lieber, R.L.; Friden, J. Functional and Clinical Significance of Skeletal Muscle Architecture. *Muscle Nerve* **2000**, *23*, 1647–1666. [CrossRef]
39. Lakens, D. Calculating and Reporting Effect Sizes to Facilitate Cumulative Science: A Practical Primer for t-Tests and ANOVAs. *Front. Psychol.* **2013**, *4*, 863. [CrossRef]

40. Fisher, M.J.; Meyer, R.A.; Adams, G.R.; Foley, J.M.; Potchen, E.J. Direct Relationship between Proton T2 and Exercise Intensity in Skeletal Muscle MR Images. *Investig. Radiol.* **1990**, *25*, 480–485. [CrossRef]
41. Sjogaard, G.; Adams, R.P.; Saltin, B. Water and Ion Shifts in Skeletal Muscle of Humans with Intense Dynamic Knee Extension. *Am. J. Physiol.* **1985**, *248*, R190–R196. [CrossRef]
42. Sinha, S.; Sinha, U.; Edgerton, V.R. In Vivo Diffusion Tensor Imaging of the Human Calf Muscle. *J. Magn. Reason. Imaging* **2006**, *24*, 182–190. [CrossRef] [PubMed]
43. Aggeloussis, N.; Giannakou, E.; Albracht, K.; Arampatzis, A. Reproducibility of Fascicle Length and Pennation Angle of Gastrocnemius Medialis in Human Gait in Vivo. *Gait Posture* **2010**, *31*, 73–77. [CrossRef] [PubMed]
44. Arampatzis, A.; Karamanidis, K.; Stafilidis, S.; Morey-Klapsing, G.; DeMonte, G.; Bruggemann, G.P. Effect of Different Ankle- and Knee-Joint Positions on Gastrocnemius Medialis Fascicle Length and EMG Activity during Isometric Plantar Flexion. *J. Biomech.* **2006**, *39*, 1891–1902. [CrossRef] [PubMed]
45. Bojsen-Moller, J.; Hansen, P.; Aagaard, P.; Kjaer, M.; Magnusson, S.P. Measuring Mechanical Properties of the Vastus Lateralis Tendon-Aponeurosis Complex in Vivo by Ultrasound Imaging. *Scand. J. Med. Sci. Sports* **2003**, *13*, 259–265. [CrossRef]
46. Sacks, R.D.; Roy, R.R. Architecture of the Hind Limb Muscles of Cats: Functional Significance. *J. Morphol.* **1982**, *173*, 185–195. [CrossRef]
47. Yagiz, G.; Akaras, E.; Kubis, H.-P.; Owen, J.A. Heterogeneous Effects of Eccentric Training and Nordic Hamstring Exercise on the Biceps Femoris Fascicle Length Based on Ultrasound Assessment and Extrapolation Methods: A Systematic Review of Randomised Controlled Trials with Meta-Analyses. *PLoS ONE* **2021**, *16*, e0259821. [CrossRef]
48. Martin, D.C.; Medri, M.K.; Chow, R.S.; Oxorn, V.; Leekam, R.N.; Agur, A.M.; McKee, N.H. Comparing Human Skeletal Muscle Architectural Parameters of Cadavers with in Vivo Ultrasonographic Measurements. *J. Anat.* **2001**, *199*, 429–434. [CrossRef]
49. Bendall, J.R. The Shortening of Rabbit Muscles during Rigor Mortis; Its Relation to the Breakdown of Adenosine Triphosphate and Creatine Phosphate and to Muscular Contraction. *J. Physiol.* **1951**, *114*, 71–88. [CrossRef]
50. Appell, H.J. Muscular Atrophy Following Immobilisation. A Review. *Sports Med.* **1990**, *10*, 42–58. [CrossRef]
51. Blazevich, A.J. Effects of Physical Training and Detraining, Immobilisation, Growth and Aging on Human Fascicle Geometry. *Sports Med.* **2006**, *36*, 1003–1017. [CrossRef]
52. Moreau, N.G.; Holthaus, K.; Marlow, N. Differential Adaptations of Muscle Architecture to High-Velocity Versus Traditional Strength Training in Cerebral Palsy. *Neurorehabilit. Neural Repair* **2013**, *27*, 325–334. [CrossRef] [PubMed]
53. Nimphius, S.; McGuigan, M.R.; Newton, R.U. Changes in Muscle Architecture and Performance during a Competitive Season in Female Softball Players. *J. Strength Cond. Res.* **2012**, *26*, 2655–2666. [CrossRef] [PubMed]